Water Radiolysis in Exchanged-Montmorillonites: The H-2 Production Mechanisms

ARTICLE *in* ENVIRONMENTAL SCIENCE & TECHNOLOGY · JULY 2013

Impact Factor: 5.33 · DOI: 10.1021/es401490t · Source: PubMed

6 AUTHORS, INCLUDING:

Chloé Fourdrin
Université Paris-Est Marne-la-Vallée
9 PUBLICATIONS **31** CITATIONS
SEE PROFILE

Christelle Latrille
Atomic Energy and Alternative Energies Com…
14 PUBLICATIONS **135** CITATIONS
SEE PROFILE

Environmental Science & Technology

Article

pubs.acs.org/est

Water Radiolysis in Exchanged-Montmorillonites: The H_2 Production Mechanisms

C. Fourdrin,*[,†] H. Aarrachi,[‖] C. Latrille,[‡] S. Esnouf,[‖] F. Bergaya,[§] and S. Le Caër[‖]

[†]Laboratoire des Solides Irradiés, UMR 7642, Ecole Polytechnique, F-91128 Palaiseau Cedex, France

[‡]Institut Rayonnement Matière de Saclay, Service Interdisciplinaire sur les Systèmes Moléculaires et les Matériaux, UMR 3299 CNRS/CEA SIS2M, Laboratoire de Radiolyse, Bat. 546, F-91191 Gif-Sur-Yvette Cedex, France

[§]Direction de l'Energie Nucléaire, Département de Physique-Chimie, Bat. 450, F-91191 Gif-Sur-Yvette Cedex, France

[‖]Centre de Recherche sur la Matière Divisée, CNRS, 1b rue de la Férollerie, F-45100 Orléans, France

Supporting Information

ABSTRACT: The radiolysis of water confined in montmorillonites is studied as a function of the composition of the montmorillonite, the nature of the exchangeable cation, and the relative humidity by following the H_2 production under electron irradiation. It is shown that the main factor influencing this H_2 production is the water amount in the interlayer space. The effect of the exchangeable cation is linked to its hydration enthalpy. When the water amount is high enough to get a basal distance higher than 1.3 nm, then a total energy transfer from the montmorillonite sheets to the interlayer space occurs, and the H_2 production measured is very similar to the one obtained in bulk water. For a basal distance smaller than 1.3 nm, the H_2 production increases with the relative humidity and thus with the water amount. Lastly, electron paramagnetic resonance measurements evidence the formation of a new defect induced by ionizing radiation. It consists of a hydrogen radical (H_2 precursor) trapped in the structure. This implies that structural hydroxyl bonds can be broken under irradiation, potentially accounting for the observed H_2 production.

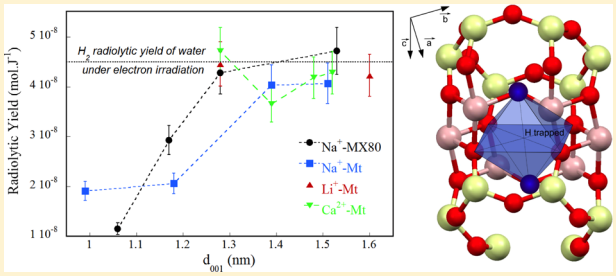

INTRODUCTION

The radiolytic decomposition of water has significant impact in the nuclear industry. H_2 radiolytically formed by water decomposition might lead to explosion and overpressure hazards in the waste package. In the context of high level radioactive waste management, heterogeneous materials such as clay minerals (or concrete) are possible candidates around the waste package. For instance, bentonite, which major component is montmorillonite (Mt—the most representative swelling clay mineral of the smectite group), is foreseen in France as backfilling material for its swelling and retention properties.[1,2] However, the significant amount of water present in the interlayer space and between the particles might enhance the H_2 production under irradiation, and despite the environmental significance, only a few studies discuss the water radiolysis in those systems.[3−9] In order to evaluate the amount of gas present around the waste, it is then necessary to perform radiolysis measurements on clay minerals for different water contents.

The stability of Mt and other clay minerals under irradiation was previously investigated: it was observed that its structure is not strongly affected after ionizing radiation in a dose range consistent with the geological storage[10−14] although point defects were evidenced in the structure of several clay minerals.[12,15,16] Long range defects such as amorphization were also reported under ballistic event but are not relevant in the case of an intact canister.[17,18]

Nevertheless, if the irradiation damages of the structure are better understood, the H_2 production by radiolysis at several relative humidities (RH) is less documented. Eriksen et al.[19] evaluated the H_2 production under α radiolysis of compacted bentonite using an ^{241}Am source and a diffusion model. They obtained a mean H_2 yield of 1.06×10^{-7} mol J^{-1}, which is of the same order of magnitude as the one obtained in water irradiated with α particles (1.2×10^{-7} mol J^{-1}).[20] However, in an other study, Brey et al. investigated a clay mineral system for which the yield obtained was significantly lower than the yield obtained in water under γ radiation.[5] In other works,[21,22] clay minerals were used as catalysts to enhance the decomposition of water or carboxylic acids under irradiation. In the present study, the H_2 yields are measured for two different Na^+-Mt with different compositions and at different RH corresponding to various adsorbed water amounts. The effect of the exchangeable cation (Li^+, Na^+, Ca^{2+}) influencing the water amount is also investigated in one Mt composition.

Received: April 8, 2013
Revised: July 2, 2013
Accepted: July 22, 2013
Published: July 22, 2013

Table 1. Chemical Compositions (%) and Structural Formulas of the Exchanged and Purified Mt[a]

	chemical composition									
sample	SiO_2	Al_2O_3	MgO	Fe_2O_3	TiO_2	Na_2O	CaO	K_2O	Li_2O	water loss
Na^+-MX80	67.78	21.73	2.29	3.88	0.16	4.07	0.01	0.07		14.59
Na^+-Mt	66.02	22.50	3.96	3.57	0.36	3.11	0.40	0.08		17.64
Li^+-Mt	66.54	23.54	3.98	3.54	0.41	0.06	0.13	0.07	1.73	9.11
Ca^{2+}-Mt	66.74	21.93	3.94	3.38	0.39	0.16	3.42	0.05		23.29

sample	structural formula
Na^+-MX80	$(Si_{4.01})_t(Al_{1.52}Mg_{0.2}Fe_{0.17})_o(OH)_2O_{10}$, $Na_{0.47}$
Na^+-Mt	$(Si_{3.83}Ti_{0.02}Al_{0.15})_t(Al_{1.50}Mg_{0.36}Fe_{0.17})_o(OH)_2O_{10}$, $Na_{0.38}Ca_{0.02}$
Li^+-Mt	$(Si_{3.91}Ti_{0.01}Al_{0.08})_t(Al_{1.54}Mg_{0.37}Fe_{0.16})_o(OH)_2O_{10}$, $Na_{0.02}Li_{0.41}$ [b]
Ca^{2+}-Mt	$(Si_{3.94}Ti_{0.01}Al_{0.03})_t(Al_{1.50}Mg_{0.35}Fe_{0.15})_o(OH)_2O_{10}$, $Na_{0.02}Ca_{0.22}$

[a]The analyses were performed at CRPG (Nancy, France) except for the Li^+-Mt sample taken from Bergaya[23]. [b]Reference 23.

MATERIALS AND METHODS

Samples Preparation. Four Mt were investigated: one from Wyoming (U.S.A.) named Na^+-MX80 and three Mt from Camp Berteau (Marocco)[23] referred as Na^+, Li^+, and Ca^{2+}-Mt. The three homoionic samples from Camp Berteau were prepared as described in Annabi-Bergaya et al.[24] Ca^{2+}-Mt and Li^+-Mt were obtained by cation exchange from Na^+-Mt with 1 N $CaCl_2$ and LiCl solutions. The Na^+-MX80 sample was purified at the DEN/DANS/DPC/SECR/L3MR laboratory (CEA Saclay, France) according to the procedure described in Gorgeon.[25] The purified samples were dehydrated at 105 °C during 24 h and then placed into four desiccators with the following RH: 0% (using silica gel), 47% (KBr saturated solution), 80% ($NaNO_3$ staurated solution), and 97% (K_2SO_4 saturated solution). The samples were placed in the desiccators at least three weeks before the experiments to ensure the complete water uptake related to the RH. Equilibrium in the desiccators was considered when stable weight was reached during at least few days. The chemical analyses (Table 1) were performed by inductively coupled plasma–atomic emission spectroscopy at CRPG (Nancy, France). The structural formulas obtained following the methodology from Caillere et al.[26] are given in Table 1. The MX80 sample presents an excess of silicium which can be linked to the presence of cristobalite as evidenced by X-ray diffraction (XRD).[27]

Irradiations Experiments and Outgassing Procedures. The samples were irradiated using 10 MeV electron pulses of a Titan Beta Inc. linear accelerator. The energy brandwith of the electrons was 15%.[28] The duration of the pulse was 10 ns and the repetition rate was set to 5 Hz in order to avoid any macroscopic heating of the sample during irradiation. The dose delivered per pulse was determined using the Fricke dosimeter (28 Gy/pulse, 1 Gy = 1 J/kg).[29] The dose determined by this method is analogous to the dose obtained using the SCN^- dosimeter in pulse radiolysis.[30] Considering the stopping power of electrons in silica, alumina, and water (ESTAR program), the doses received by the solid and the water were considered to be the same; therefore no dose correction was performed. The dose was calculated with respect to the whole clay mineral/water system. Each sample was irradiated four times at 200 kGy in order to reach a cumulative dose of 800 kGy. Prior to irradiation, the samples (approximately 150 mg) were placed in a Pyrex glass ampule (10.5 mL), which was outgassed at 3 mbar and subsequently filled with 1.2 bar of argon 4.0. This operation was repeated three times before each irradiation step and the ampule was subsequently tightly closed. In order to evidence the effects induced by ionizing radiation, for each irradiated sample a nonirradiated sample underwent the same outgassing procedure and was used as a reference. This reference sample was used to determine the initial water content by TGA (Thermogravimetric analysis) and the initial basal distance by XRD. Furthermore, the Na^+-MX80 (RH = 80%) sample was irradiated at liquid nitrogen temperature in sealed Pyrex tubes for electron paramagnetic resonance measurements. In this configuration, the estimated deposited dose was 20 Gy/pulse, and the sample was irradiated at a total dose of 140 kGy (with an error of 20%).

Analytical Methods. The changes of the interlayer water amount were investigated by XRD. Powder X-ray patterns were recorded with an Inel diffractometer equipped with a curve detector CPS120 allowing a simultaneous acquisition between 1.3° and 110° and a Co Kα (1.78897 Å) tube operating at 30 kV and 30 mA. The samples were placed under a mylar film and the position of the (*001*) peak was recorded after 10 min acquisition in order to avoid any modification of the water content in the sample.

TGA measurements were performed with a NETZSCH STA 449 F3 Jupiter. The samples (approximately 50 mg) were placed in alumina crucibles and heated from 20 to 300 °C (at 10 °C min^{-1}) under an helium flux of 70 mL min^{-1}. The main water losses occurred between 60 and 140 °C.

In order to monitor the evolution of H_2 produced during irradiation, the gas contained in the ampule was analyzed by gas chromatography (μGC-R3000 SRA instrument) using ultra-high-purity argon (argon 6.0) as the carrier gas. Prior to the acquisition of the chromatogram, the gas contained in the ampule was mixed with argon at 1.2 bar for five minutes. The estimated error in the gas measurement is less than 10%.

EPR spectra were acquired on a X-Band Bruker spectrometer with a 100 kHz field modulation, a 20 μW microwave power, and a 0.1 mT amplitude modulation. The microwave frequency was measured with a frequency counter. The spectra were acquired at 104 K with a nitrogen flow device.

RESULTS AND DISCUSSION

Characterization of the Mt before Irradiation. The four Mt samples were investigated at different RH by TGA and XRD. The basal spacings d_{001} observed before irradiation (Table 2) are in good agreement with previous results reported on similar systems.[31] It is well-known that the basal spacing d_{001} increases with the RH. Typical basal spacings are 1.3, 1.5, and 1.8 nm for respectively 1, 2, and 3 water layers in the interlayer space.[32] Due to our experimental conditions, the d_{001} was determined using the Bragg peak position. However, it should

dx.doi.org/10.1021/es401490t | Environ. Sci. Technol. 2013, 47, 9530–9537

Table 2. Basal Spacings d_{001} (nm) Determined by XRD and Water Amounts (%) Determined by Thermogravimetric Measurements[a]

	d_{001} (nm)							
	Na^+-MX80		Na^+-Mt		Li^+-Mt		Ca^{2+}-Mt	
RH (%)	bi	ai	bi	ai	bi	ai	bi	ai
0	1.1	nd	1.0	nd	1.3	nd	1.3	nd
47	1.2	1.1	1.2	1.2	nd	nd	1.4	1.4
80	1.3	1.2	1.4	1.4	nd	nd	1.5	1.4
97	1.5	1.5	1.5	1.5	1.6	1.6	1.5	1.5
	Water Amount Determined by TGA (%)[b]							
	Na^+-MX80		Na^+-Mt		Li^+-Mt		Ca^{2+}-Mt	
RH (%)	bi	ai	bi	ai	bi	ai	bi	ai
0	2.9	nd	4.4	3.7	nd	10.6	8.5	nd
47	5.8	6.2	11	9.7	nd	nd	16.9	17.3
80	13.5	12.1	18.1	17.1	nd	nd	22.6	20.8
97	21.4	18.3	25.7	21.5	30.5	23.8	23.6	21.6

[a]The error on the d_{001} value is estimated at 0.1 nm.[33] The error on the water amounts is estimated at 1%. bi stands for before irradiation; ai stands for after irradiation; nd stands for not determined. [b]Cation hydration enthalpy values (kJ mol^{-1})[37]: Na^+-MX80, −405; Na^+-Mt, −405; Li^+-Mt, −520; Ca^{2+}-Mt, −1650.

be pointed out that using this methodology induces an error (about 1 Å) on the value of the basal spacing as was evidenced by Holmboe et al.[33]

Although all the samples were submitted to the same thermal treatment, the Ca^{2+}-Mt and Li^+-Mt retain more water in the interlayer space than the Na^+-Mt and Na^+-MX80. The water amount obtained by TGA measurements before irradiation confirms this result (Table 2). In Mt, several types of water must be distinguished: the structural −OH bonds within the octahedral sheets, the interlayer water which is observed by XRD; the water molecules chemisorbed to the surface of the particles and present in the mesopores (ranging from 2 to 50 nm); and the free water molecules which lay in the mesopores and are observed at high RH (>90%).[34]

The proportion of the different types of water are difficult to assess for each RH, but for a d_{001} close to 1 nm, the water types present in the system are the structural hydroxyl groups and the chemisorbed water molecules. At higher water loading (and thus for higher RH), it has been demonstrated that the water molecules predominantly lie in the interlayer space for the three exchangeable cations.[35,36] Therefore, in this study, the radiolytic yields will be discussed as a function of the basal spacing, and the TGA measurements will be used to determine the total water amount present in the system (except the structural −OH bonds within the sheets).

Effect of the Exchangeable Cation on H_2 Radiolytic Yield. The evolution of the H_2 production as a function of the dose and of the RH is presented in Figure 1 for the Na^+-MX80 sample. The H_2 production evolves linearly with the dose indicating that no saturation phenomena occur within this dose range. The slight decrease observed at the highest cumulated dose is probably related to the important water loss under irradiation as observed by TGA (Table 2).

The calculated H_2 radiolytic yields are presented in Table 3. Two main tendencies are noticed: on one hand, for both Na^+-MX80 and Na^+-Mt, the yield increases with the RH. On the other hand, the Ca^{2+}-Mt exhibits a different behavior: the yield is almost constant for all RH. Although more data points are

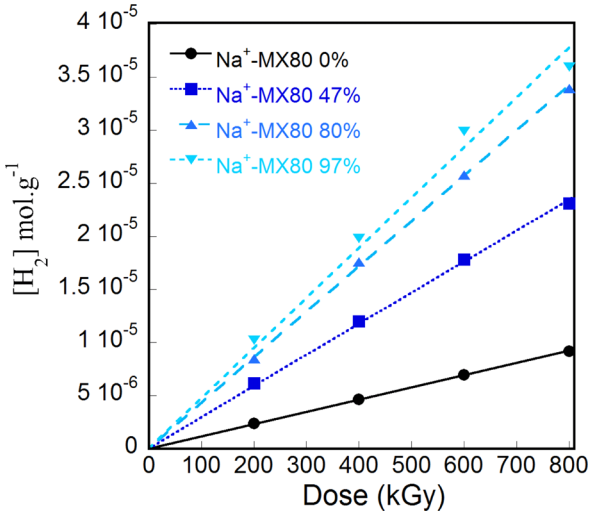

Figure 1. H_2 production (mol g^{-1}) for the Na^+-MX80 sample as a function of the cumulated dose for various RH. The points are the experimental data, and the lines correspond to the linear fits.

required for the Li^+-Mt, the same behavior as for the Ca^{2+}-Mt can be expected, since both samples possess a high initial d_{001} at low RH. Since the initial water amounts are related to the hydration enthalpy of the exchangeable cation (Table 2),[37] the radiolytic yields were also plotted as a function of the initial d_{001} (Figure 2). From Figure 2, two behaviors can be depicted: when d_{001} is smaller than 1.3 nm, the radiolytic yield increases with the basal spacing. When d_{001} is higher than 1.3 nm, then the radiolytic yield remains constant with a value similar to the one obtained in bulk water (4.5×10^{-8} mol J^{-1} under electron irradiation).[38,39] Therefore, when the interlayer space is at least filled with one water layer, the maximal radiolytic yield is reached. Besides, when the d_{001} distance is lower than 1.3 nm, the interlayer space is holding either 0 or 1 water layer. With increasing RH (for $1 < d_{001} < 1.3$ nm), the basal distance expands with the amount of interlayer spaces filled with one water layer. Consequently, the dihydrogen production is related to the proportion of interlayer space filled with one water layer.

At this point, it is also necessary to point out that the radiolytic yields obtained when the d_{001} value is higher than 1.3 nm are calculated using the total mass of the clay mineral−water system. This implies that the yield calculated from the water amount only is higher than in pure water. This evidence an energy transfer from the clay mineral layer to the interlayer space under irradiation.

The modifications of the basal spacing and water loading determined by XRD and TGA under irradiation are given in Table 2. After irradiation, a strong dehydration is observed by TGA and the basal spacings are also affected. Those results demonstrate that the dehydration process is significant, mainly for the highest RH, even when working with a low pulse frequency of the linear accelerator (5 Hz).

The competition between dehydration and H_2 production can be examined more carefully in the most striking case, i.e. at the highest RH. For instance, in the case of the Na^+-MX80 sample at RH = 97%, the H_2 production is 3.7×10^{-2} mol kg^{-1} after a 800 kGy irradiation, while the number of desorbed water molecules is 1.72 mol kg^{-1} as estimated from TGA measurements (Table 2). Therefore in this case, for each H_2 molecule produced, approximately 50 water molecules are removed from the clay mineral. This water desorption has already been

dx.doi.org/10.1021/es401490t | Environ. Sci. Technol. 2013, 47, 9530−9537

Table 3. H_2 Radiolytic Yield (mol/J)[a]

RH (%)	Na^+-MX80	Na^+-Mt	Li^+-Mt	Ca^{2+}-Mt
0	$(1.2 \pm 0.1) \times 10^{-8}$	$(1.9 \pm 0.2) \times 10^{-8}$	$(4.5 \pm 0.5) \times 10^{-8}$	$(4.7 \pm 0.5) \times 10^{-8}$
47	$(2.9 \pm 0.3) \times 10^{-8}$	$(2.1 \pm 0.2) \times 10^{-8}$	nd	$(3.7 \pm 0.4) \times 10^{-8}$
80	$(4.3 \pm 0.4) \times 10^{-8}$	$(4.0 \pm 0.4) \times 10^{-8}$	nd	$(4.2 \pm 0.4) \times 10^{-8}$
97	$(4.7 \pm 0.5) \times 10^{-8}$	$(4.1 \pm 0.4) \times 10^{-8}$	$(4.2 \pm 0.4) \times 10^{-8}$	$(4.2 \pm 0.4) \times 10^{-8}$

[a]nd stands for not determined. The error is estimated at 10%.

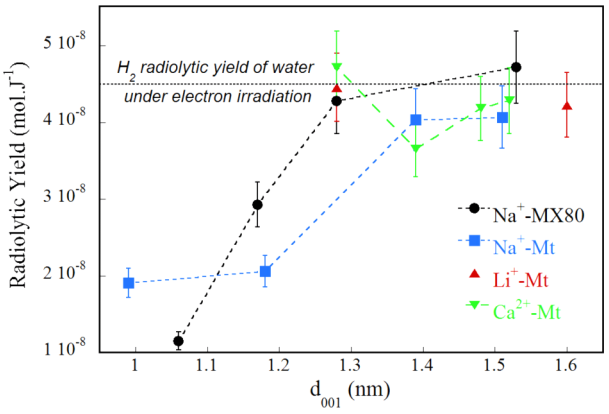

Figure 2. H_2 radiolytic yields as a function of the initial d_{001}. The error on the radiolytic yield is estimated at 10%.

evidenced in the case of the mesoporous silica SBA-15 irradiated by 10 MeV electron pulses.[40] The desorption can be linked to a slight increase of the temperature during irradiation even if no macroscopic heating was observed at the end of it. Besides, it can also be triggered by low energy secondary electrons produced during irradiation, as evidenced in a study from Petrik and Kimmel.[41]

Characterization of the Trapped Hydrogen Radical (H•). EPR spectroscopy was used to observe the possible trapping of H• (a precursor in the H_2 formation) in the clay mineral layer. For instance, trapped hydrogen radicals were previously observed in natural and synthetic kaolinite under ionizing radiation.[42] They were also reported in a broad range of materials such as zeolites, silasequioxane cages or quartz.[42−49] In the present study, the signals observed in Figure 3a can be assigned to two types of defects. The broad asymmetric line detected around $g = 2$ (0.33 T) is attributed to

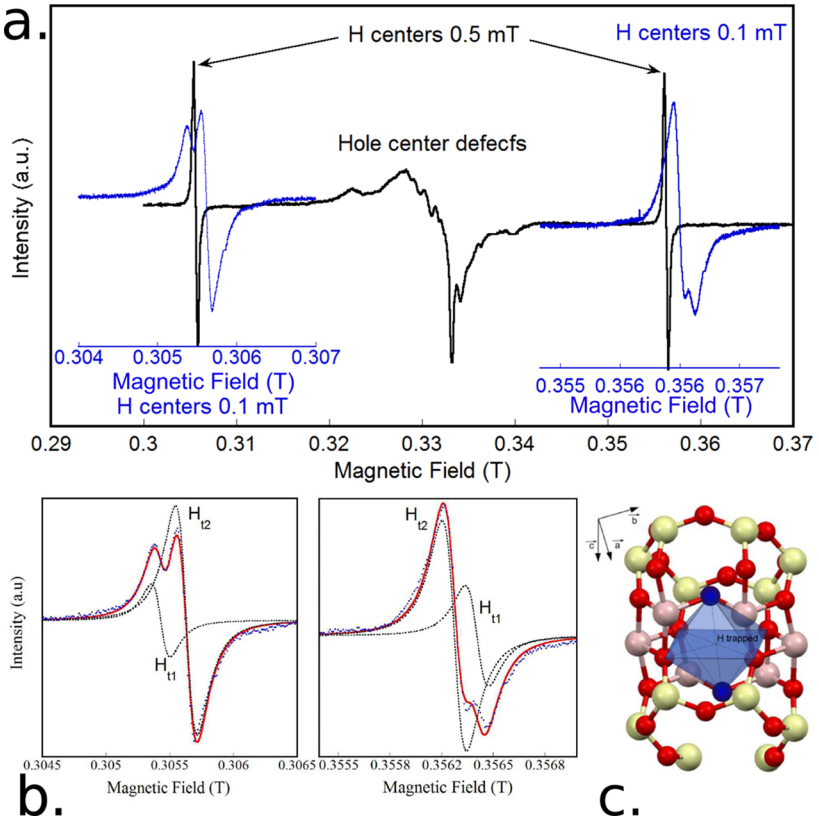

Figure 3. (a) EPR spectra of the Na^+-MX80 sample at ambient RH after an irradiation of 140 kGy at 77 K. The signals were acquired at 104 K at two different modulations, 0.1 mT and 0.5 mT, respectively. The 0.1 mT signals are expanded 11 times with respect to the magnetic field. (b) Adjustments of EPR spectra acquired at 0.1 mT and 104 K. Dots: experimental spectrum. Plain red line: complete adjustment. Dotted lines: adjustments for the two defects H_{t1} and H_{t2}. (c) Trapping site for the hydrogen radical. The structure is based on the results of X-ray diffraction patterns simulations obtained by Viani et al.[53] The unit cell parameters used are as follows: $a = 5.18$ Å, $b = 8.98$ Å, $c = 15$ Å in the $P1$ space group. In this structure, the crystallographic positions of the trap are as follows: $x = 0.3753$; $y = 0.5$; $z = 0.2214$. Oxygen, aluminum, and silicon atoms are represented in red, pink, and yellow, respectively; oxygen atoms of the OH groups are represented in blue.

dx.doi.org/10.1021/es401490t | Environ. Sci. Technol. 2013, 47, 9530−9537

the presence of overlapping oxygen hole centers;[11,50] whereas the doublet separated by ca. 51 mT is related to the trapped hydrogen radicals.[42] The whole spectra was acquired at a modulation of 0.5 mT, and in order to resolve the components of the trapped hydrogen spectra, the signals were acquired at a modulation of 0.1 mT (Figure 3a,b).

The EPR spectra at 0.1 mT were simulated by the ZFSFIT program.[51] The results of the adjustments are presented in Figure 3b. The obtained values ($gH_{t1}H_{t2}$ = 2.00248, AH_{t1} = 1427.2 MHz, AH_{t2} = 1417.6 MHz) are in good agreement with previous values reported in the literature.[42,47,52] The hyperfine constant A for the first Mt defect (H_{t1}) is larger than the second one (H_{t2}), indicating that the electronic density at the nucleus is larger and therefore that the hydrogen atom is trapped in a smaller cavity.

Besides, the obtained values are close to the ones reported by Toriyama et al. in kaolinite.[42] By analogy with the trapped hydrogen (H_t) in Ar gas and quartz, the authors proposed two trapping sites for the H_{t1} and H_{t2} (outer and inner trapped hydrogen doublet, respectively) in kaolinite. Both sites are formed by a cage of six oxygen atoms surrounded by six aluminum ions. They are distinguished by their behavior with increasing dose and the presence of impurities. It is possible to propose similar traps in Mt in the octahedral sheet. The presence of two sites is justified by the substitution of Al atoms by Mg (or Fe) atoms which induces a modification of the trap geometry. The traps are composed of six oxygen atoms, and the mean distance between their center and the oxygen atoms is 2.25 Å (Figure 3c).[53] This value is similar in kaolinite (2.23 Å) and in quartz (2.20 Å).[42] Mt is a dioctahedral clay mineral, meaning that one of every three octahedral site is vacant. The trapping site for the $H^\bullet$ is the center of this third octahedral site.

Mechanisms for the H_2 Formation. H_2 formation is always measured under irradiation at different RH, even for the driest samples (Table 3). The H_2 yields are in good accordance with the only value reported in the literature by Eriksen et al.[19] (roughly 10^{-7} mol J^{-1} using an α source). The fact that the H_2 radiolytic yields observed in Figure 2 are of the same order of magnitude in our samples as in pure water ($4.5.10^{-8}$ mol J^{-1}) demonstrates that the energy deposited in the clay layer is transferred to the interlayer space.[54] In the case of water adsorbed on different oxides, Petrik et al.[54] proposed a model in which the energy migrates in the material under the form of an exciton, and they evaluate the migration distance at 5 nm. However, in Mt, water molecules predominantly lie between each clay mineral layer. Knowing that a single clay layer has a height of 0.96 nm, electrons and holes produced under irradiation in the clay mineral layer can migrate directly toward the interlayer water molecules.

The study of water radiolysis in Mt can be compared to the radiolysis in other silicate systems: zeolites[55] and silica.[45,56−58] In the case of dried porous silica, the surface of the pores contain hydroxyl groups from which the dihydrogen production arises.[40] If silica is hydrated, water molecules are adsorbed on surface hydroxyl groups and act then as exciton trapping sites.[6,40,57] In our case, the surface of the Mt layer is more similar to zeolites with no hydroxyl groups and a negative charge which is counter balanced by charge compensating ions in the interlayer space.

Besides, contrary to silica, materials such as γ-alumina, zeolites, and clay minerals are known to exhibit ionic processes under ionizing radiation.[6] The radiolytic events are known in zeolites,[6] and similar reaction mechanisms can be expected in clay minerals.

First, ionization of the clay minerals leads to the production of a hole and an electron. The electron and the hole can either recombine or be trapped in the matrix. Electrons which are not trapped in the clay mineral layer can be transferred from the ionized layer to the interlayer space where they are hydrated by water molecules (eq 1).[59]

$$e^- \xrightarrow{H_2O} e^-_{aq} \quad (1)$$

Those hydrated electrons are known to lead to H_2 production[60] (eq 2).

$$e^-_{aq} + e^-_{aq} \rightarrow H_2 + 2OH^- \quad (2)$$

In the case of H_2 formation in zeolites, Nakashima and Aratono[55] suggested that the surface anionic oxygen atoms are trapping sites for the positives holes produced under irradiation. In clay minerals, hole trapping by oxygen atoms of the structure was widely studied but the precise location of the centers in several clay minerals is difficult to ascertain.[11,15,16,61] These defects are observed by EPR around g = 2.[15,62] For instance, three types of holes trapped on oxygen atoms were evidenced in kaolinite, and their stability depends on the environment of the concerned oxygen atom.[15,50] In Mt, two types of holes trapped on oxygen atoms were reported, but their exact position in the structure remains unclear.[11] Holes that are not trapped in the clay mineral layer can also migrate to the surface of the layer giving rise to another source of molecular H_2:

$$H_2O + h^+ \rightarrow H^+ + OH^\bullet \quad (3)$$

$$H^+ + e^-_{aq} \rightarrow H^\bullet + H_2O \quad (4)$$

$$H^\bullet + e^-_{aq} \rightarrow H_2 + OH^- \quad (5)$$

$$H^\bullet + H^\bullet \rightarrow H_2 \quad (6)$$

Therefore, all these possible mechanisms imply that H_2 can only be efficiently produced when the charges are transferred from the layer to the interlayer space, and for that purpose, water molecules have to interact with the siloxane surface. At high water content, direct water radiolysis must also be considered.

It is worth noting here that the electron, although being a strong reducer, is not able to reduce alkali cations or metal-alkali cations,[63,64] meaning that the cations in the interlayer space will not be reduced under irradiation. Besides, it was not possible here to invetigate the possible oxidation or reduction of the iron present in the octahedral layer. Other studies discuss the fate of iron and its impact on radiolysis products such as H_2O_2.[4,33,65]

In the case of the Ca^{2+}- and the Li^+-Mt, the H_2 radiolytic yields remain constant within the water content range studied here; while in the case of the sodium samples, the H_2 yield increases with the water content. From Table 2, it appears clearly that there is always at least one water layer in the Ca^{2+}- and Li^+-Mt samples, whereas this is only the case at the two highest RH for the Na^+-Mt and Na^+-MX80. This proves that the electrons are even more efficiently transferred to the interlayer space that the water amount is increased. At low RH, it was proven by molecular simulation[66] in the case of Li^+-, Na^+-, and K^+-Mt that water adsorption is driven by the

dx.doi.org/10.1021/es401490t | Environ. Sci. Technol. 2013, 47, 9530−9537

hydration enthalpy of the interlayer exchangeable cation. Water adsorption increases then with the cation−water hydration energy. At high water content, water molecules are adsorbed on the clay mineral surface leading to the formation of an extensive H bond network. Other calculations[67] have shown that the formation of H bonds with the oxygen atoms of the siloxane surfaces occurs for a d_{001} value of 1.3 nm. This result is in agreement with our experimental findings (Figure 2). When d_{001} is smaller than 1.3 nm, the H_2 radiolytic yield increases with the basal spacing, and thus with the proportion of interlayer space filled with one water layer. When the d_{001} value is greater than 1.3 nm, the H_2 radiolytic yield remains almost constant and its value is similar to the one obtained in bulk water. In this latter case, the H bond network is extended[64,68,69] and enables a total energy transfer from the layer of the clay mineral to the interlayer space. The H_2 production is then driven by the water content and therefore by the hydration enthalpy of the exchangeable cations (Table 2). Lastly, a slight difference in the H_2 production in the case of the two sodium exchanged Mt is evidenced in Figure 2. Both samples exhibit globally the same behavior, proving that the hydration enthalpy of the cation is the most important parameter and that the nature of the structure has only a marginal influence on the H_2 production.

Under irradiation, the possible sources for the hydrogen atom trapped in Mt are the O−H bond inside the clay mineral layer (Figure 3c) and the hydrogen radicals formed upon decomposition of the water molecule in the interlayer space.[4] The structural hydroxyl groups within the sheets appear to be the most plausible source for hydrogen radicals observed by EPR spectroscopy.[48] Indeed, the oxygen atom from the O−H bond is one of the six oxygen atoms constituting the trap. Therefore the migration distance after the O−H bond cleavage is low and the geometrical changes are weak (Figure 3c). Moreover, this defect was also observed in kaolinite, which is a non swelling clay mineral and therefore does not exhibit interlayer water molecules.[42] The structural hydroxyl bond cleavage leads to the formation of an hole center on an oxygen atom between two Al atoms (Al−O^-Al center).[15,62]

Those results suggest the following reaction, in accordance with Milosavljevic and Thomas:[70]

$$\mathrm{Al{-}OH{-}Al} \xrightarrow{\text{radiation}} \mathrm{Al{-}O^{-}{-}Al} + \mathrm{H^{+}} \qquad (7)$$

This could then lead to H_2 production as described in eqs 4−6.

In this study, we reported direct measurements of the H_2 production from Mt radiolysis irradiated at several RH. It is observed that this production is non-negligible even for the driest samples at low doses. Therefore, H_2 will be produced around the waste package in the clay buffer. The amount of H_2 produced must be taken in account in the models developed to predict the gas diffusion in the clay layer and to avoid overpressure around the waste packages. Reaction mechanisms are proposed to account for this H_2 formation. It is also suggested that the hydroxyl bonds inside this clay mineral can be broken under irradiation.

■ ASSOCIATED CONTENT

Supporting Information

The attenuated total reflection infrared spectroscopy (ATR-IR) characterization of montmorillonite before irradiation is presented and analyzed. The results obtained by this spectroscopy are in good agreement with the manuscript results. This material is available free of charge via the Internet at http://pubs.acs.org.

■ AUTHOR INFORMATION

Corresponding Author

*Phone: 0033 1 69334566; fax: 0033 1 69334554; e-mail: chloe.fourdrin@polytechnique.edu.

Notes

The authors declare no competing financial interest.

■ ACKNOWLEDGMENTS

The authors thank J. Ly for providing the Na^+-MX80 purified sample. We also thank V. Dauvois and B. Boizot for helpful discussion.

■ REFERENCES

(1) Pusch, R.; Karnland, O. Physico chemical stability of smectite clays. *Eng. Geol.* **1996**, *41*, 73−85. ISMES 3rd International Workshop on Clay Barriers—Thermomechanics of Clays and Clay Barriers, Bergamo, Italy, Oct 22−24, 1993.

(2) Pusch, R.; Kasbohm, J.; Thao, H. T. M. Chemical stability of montmorillonite buffer clay under repository-like conditions—A synthesis of relevant experimental data. *Appl. Clay. Sci.* **2010**, *47*, 113−119. Workshop on Long-term Performance of Smectitic Clays Embedding Canisters with Highly Radioactice Waste, IDEON Sci Pk, Lund, Sweden, Nov 26−28, 2007.

(3) Eriksen, T.; Lind, J. *Formation of molecular hydrogen by radiolysis in hydrated bentonite*; Technical Report, (SKB, Sweden), 1979.

(4) Gournis, D.; Mantaka-Marketou, A.; Karakassides, M.; Petridis, D. Effect of gamma-irradiation on clays and organoclays: a Mossbauer and XRD study. *Phys. Chem. Miner.* **2000**, *27*, 514−521.

(5) Brey, R.; Rodriguez, R.; Harmon, J.; Winston, P. Investigation of irradiated soil byproducts. *Waste Manage.* **2001**, *21*, 581−588.

(6) Thomas, J. K. Physical aspects of radiation-induced processes on SiO(2), gamma-Al(2)O(3), zeolites, and clays. *Chem. Rev.* **2005**, *105*, 1683−1734.

(7) Bouniol, P.; Bjergbakke, E. A comprehensive model to describe radiolytic processes in cement medium. *J. Nucl. Mater.* **2008**, *372*, 1−15.

(8) Holmboe, M.; Wold, S.; Jonsson, M.; Garcia-Garcia, S. Effects of gamma-irradiation on the stability of colloidal Na(+)-montmorillonite dispersions. *Appl. Clay. Sci.* **2009**, *43*, 86−90.

(9) Holmboe, M.; Norrfors, K. K.; Jonsson, M.; Wold, S. Effect of gamma-radiation on radionuclide retention in compacted bentonite. *Radiat. Phys. Chem.* **2011**, *80*, 1371−1377.

(10) Plotze, M.; Kahr, G.; Stengele, R. Alteration of clay minerals—gamma-irradiation effects on physicochemical properties. *Appl. Clay Sci.* **2003**, *23*, 195−202. Workshop on Clay Microstructure, Lund, Sweden, Oct 15−17, 2002.

(11) Sorieul, S.; Allard, T.; Morin, G.; Boizot, B.; Calas, G. Native and artificial radiation-induced defects in montmorillonite. An EPR study. *Phys. Chem. Miner.* **2005**, *32*, 1−7.

(12) Sorieul, S.; Allard, T.; Wang, L. M.; Grambin-Lapeyre, C.; Lian, J.; Calas, G.; Ewing, R. C. Radiation-stability of smectite. *Environ. Sci. Technol.* **2008**, *42*, 8407−8411.

(13) Fourdrin, C.; Balan, E.; Allard, T.; Boukari, C.; Calas, G. Induced modifications of kaolinite under ionizing radiation: an infrared spectroscopic study. *Phys. Chem. Miner.* **2009**, *36*, 291−299.

(14) Allard, T.; Balan, E.; Calas, G. In *Handbook of Clay Science—Part A: Fundamentals*; Bergaya, F., Lagaly, G., Eds.; Developments in Clay Science, 2nd ed., Vol. 5; Elsevier: 2013; pp 127−138.

(15) Clozel, B.; Allard, T.; Muller, J. Nature and stability of radiation-induced defects in natural kaolinites—new results and a reappraisal of published works. *Clay. Clay. Miner.* **1994**, *42*, 657−666.

(16) Morichon, E.; Allard, T.; Beaufort, D.; Patrier, P. Evidence of native radiation-induced paramagnetic defects in natural illites from

unconformity-type uranium deposits. *Phys. Chem. Miner.* **2008**, *35*, 339−346.
(17) Fourdrin, C.; Allard, T.; Monnet, I.; Menguy, N.; Benedetti, M.; Calas, G. Effect of radiation-induced amorphization on smectite dissolution. *Environ. Sci. Technol.* **2010**, *44*, 2509−2514.
(18) Allard, T.; Calas, G. Radiation effects on clay mineral properties. *Appl. Clay. Sci.* **2009**, *43*, 143−149.
(19) Eriksen, T.; Christensen, H.; Bjergbakke, E. Hydrogen production in alpha-irradiated bentonite. *J. Radioanal. Nucl. Ch.* **1987**, *116*, 13−25.
(20) Pastina, B.; LaVerne, J. Effect of molecular hydrogen on hydrogen peroxide in water radiolysis. *J. Phys. Chem. A* **2001**, *105*, 9316−9322.
(21) Negron-Mendoza, A.; Ramos-Bernal, S. Radiolysis of carboxylic acids adsorbed in clay minerals. *Radiat. Phys. Chem.* **1998**, *52*, 395−399. Proceedings of the 10th International Meeting on Radiation Processing.
(22) Cecal, A.; Hauta, O.; Macovei, A.; Popovici, E.; Rusu, I.; Puica, N. M. Hydrogen yield from water radiolysis in the presence of some pillared clays. *Rev. Roum. Chim.* **2008**, *53*, 875+.
(23) Bergaya, F. Ph.D. Thesis, Orleans, 1971.
(24) Annabi-Bergaya, F.; Cruz, M.; Gatineau, L.; Fripiat, J. Adsortion of alcohols by smectites: I. Distinction between internal and external surfaces. *Clay. Miner.* **1979**, *14*, 249−258.
(25) Gorgeon, L. Contribution to the physico-chemical modelling of the retention of long-lived radionuclides by clay minerals. Ph.D. Thesis, Paris XI, 1994.
(26) Caillere, S.; Henin, S.; Rautureau, M. In *Clay Mineralogy*, 2nd ed.; Masson: 1982; p 384.
(27) Brindley, G. W., Brown, G., Eds. In *Crystal Structure of Clay Minerals and Their Identification*; Monograph, Mineralogical Society; Brookfield Publishing Co.: 1980.
(28) Mialocq, J.; Hickel, B.; Baldacchino, G.; Juillard, M. The radiolysis project of CEA. *J. Chim. Phys. Phys.-Chim. Biol.* **1999**, *96*, 35−43. Conference on the Development and Current Problems in Radiation Chemistry (JECR-1998), Bonascre, France, Jun 21−26, 1998.
(29) Fricke, H.; Hart, J. E. In *Radation Dosimetry*, 2nd ed.; Attix, F. H., Roesch, W. C., Eds.; Academic Press: New York and London, 1966; Vol. *2*; p 167.
(30) Milosavljevic, B. H.; LaVerne, J. A. Pulse radiolysis of aqueous thiocyanate solution. *J. Phys. Chem. A* **2005**, *109*, 165−168.
(31) Ferrage, E.; Lanson, B.; Sakharov, B.; Drits, V. Investigation of smectite hydration properties by modeling experimental X-ray diffraction patterns: Part I. Montmorillonite hydration properties. *Am. Mineral.* **2005**, *90*, 1358−1374.
(32) Lagaly, G. In *Handbook of Clay Science—Part A: Fundamentals*; Bergaya, F., Lagaly, G., Eds.; Developments in Clay Science, 2nd ed., Vol. 5; Elsevier: 2013; pp 245−328.
(33) Holmboe, M.; Wold, S.; Jonsson, M. Porosity investigation of compacted bentonite using XRD profile modeling. *J. Contam. Hydrol.* **2012**, *128*, 19−32.
(34) Salles, F.; Beurroies, I.; Bildstein, O.; Jullien, M.; Raynal, J.; Denoyel, R.; Damme, H. V. A calorimetric study of mesoscopic swelling and hydration sequence in solid Na-montmorillonite. *Appl. Clay. Sci.* **2008**, *39*, 186−201.
(35) Norrish, K. The swelling of montmorillonite. *Discuss. Faraday Soc.* **1954**, *18*, 120−134.
(36) Salles, F.; Bildstein, O.; Douillard, J. M.; Jullien, M.; Raynal, J.; Van Damme, H. On the cation dependence of interlamellar and interparticular water and swelling in smectite clays. *Langmuir* **2010**, *26*, 5028−5037.
(37) Atkins, P.; De Paula, J. In *Physical Chemistry*, 6th ed.; Oxford Unniversity Press: Oxford, 2000; p 926.
(38) Schwarz, H. A.; Losee, J. P.; Allen, A. O. Hydrogen yields in the radiolysis of aqueous solutions1. *J. Am. Chem. Soc.* **1954**, *76*, 4693−4694.
(39) Pastina, B.; LaVerne, J. A.; Pimblott, S. M. Dependence of molecular hydrogen formation in water on scavengers of the precursor to the hydrated electron. *J. Phys. Chem. A* **1999**, *103*, 5841−5846.
(40) Brodie-Linder, N.; Le Caer, S.; Alam, M. S.; Renault, J. P.; Alba-Simionesco, C. H(2) formation by electron irradiation of SBA-15 materials and the effect of Cu(II) grafting. *Phys. Chem. Chem. Phys.* **2010**, *12*, 14188−14195.
(41) Petrik, N. G.; Kimmel, G. A. Hydrogen bonding, H-D exchange, and molecular mobility in thin water films on TiO_2 (110). *Phys. Rev. Lett.* **2007**, *99*, 196103.
(42) Toriyama, K.; Lund, A.; Okazaki, M. Trapped hydrogen atoms radiolytically formed in natural and synthetic kaolinites: an electron paramagnetic resonance study. *Phys. Chem. Chem. Phys.* **2000**, *2*, 4697−4701.
(43) Balling, L. C.; Pipkin, F. M. Gyromagnetic ratios of hydrogen, tritium, free electrons, and Rb^{85}. *Phys. Rev.* **1965**, *139*, A19−A26.
(44) Sasamori, R.; Okaue, Y.; Isobe, T.; Matsuda, Y. Stabilization of atomic hydrogen in both solution and crystal at room temperature. *Science* **1994**, *265*, 1691−1693.
(45) Liu, X.; Zhang, G.; Thomas, J. K. Spectroscopic studies of electron and hole trapping in zeolites: formation of hydrated electrons and hydroxyl radicals. *J. Phys. Chem. B* **1997**, *101*, 2182−2194.
(46) Paech, M.; Stoesser, R. Scavenger assisted trapping of atomic hydrogen in Si_8O_{12}-cages. *J. Phys. Chem. A* **1997**, *101*, 8360−8365.
(47) Gross, B.; Dilger, H.; Scheuermann, R.; Paech, M., M.ch; Roduner, E. Electron paramagnetic resonance study of the dynamics of H and D atoms trapped in substituted silasesquioxane cages. *J. Phys. Chem. A* **2001**, *105*, 10012−10017.
(48) Chemerisov, S.; Trifunac, A. Probing nanoconfined water in zeolite cages: H atom dynamics and spectroscopy. *Chem. Phys. Lett.* **2001**, *347*, 65−72.
(49) Chemerisov, S.; Werst, D.; Trifunac, A. Formation, trapping and kinetics of H atoms in wet zeolites and mesoporous silica. *Radiat. Phys. Chem.* **2001**, *60*, 405−410. International symposium on prospects for application of radiation.
(50) Allard, T.; Balan, E.; Calas, G.; Fourdrin, C.; Morichon, E.; Sorieul, S. Radiation-induced defects in clay minerals: A review. *Nucl. Instrum. Meth. B* **2012**, *277*, 112−120. Basic research on ionic-covalent materials for nuclear applications.
(51) Morin, G.; Bonnin, D. Modeling EPR powder spectra using numerical diagonalization of the spin Hamiltonian. *J. Magn. Reson.* **1999**, *136*, 176−199.
(52) Stoll, S.; Ozarowski, A.; Britt, R. D.; Angerhofer, A. Atomic hydrogen as high-precision field standard for high-field EPR. *J. Magn. Reson.* **2010**, *207*, 158−163.
(53) Viani, A.; Gaultieri, A.; Artioli, G. The nature of disorder in montmorillonite by simulation of X-ray powder patterns. *Am. Mineral.* **2002**, *87*, 966−975.
(54) Petrik, N.; Alexandrov, A.; Vall, A. Interfacial energy transfer during gamma radiolysis of water on the surface of ZrO_2 and some other oxides. *J. Phys. Chem. B* **2001**, *105*, 5935−5944.
(55) Nakashima, M.; Aratono, Y. Radiolytic hydrogen gas formation from water adsorbed on type A zeolites. *Radiat. Phys. Chem.* **1993**, *41*, 461−465.
(56) Le Caer, S.; Rotureau, P.; Brunet, F.; Charpentier, T.; Blain, G.; Renault, J.; Mialocq, J. Radiolysis of confined water: Hydrogen production at a high dose rate. *ChemPhysChem* **2005**, *6*, 2585−2596.
(57) Rotureau, P.; Renault, J. P.; Lebeau, B.; Patarin, J.; Mialocq, J.-C. Radiolysis of confined water: molecular hydrogen formation. *ChemPhysChem* **2005**, *6*, 1316−1323.
(58) Le Caer, S. Water radiolysis: Influence of oxide surfaces on H2 production under ionizing radiation. *Water* **2011**, *3*, 235−253.
(59) Musat, R. M.; Cook, A. R.; Renault, J.-P.; Crowell, R. A. Nanosecond pulse radiolysis of nanoconfined water. *J. Phys. Chem. C* **2012**, *116*, 13104−13110.
(60) Pastina, B.; LaVerne, J. A. Scavenging of the precursor to the hydrated electron by the selenate ion. *J. Phys. Chem. A* **1999**, *103*, 209−212.

(61) Morichon, E.; Allard, T.; Beaufort, D.; Quirt, D. An EPR study of native radiation-induced paramagnetic defects in sudoite (di-trioctahedral Al-Mg chlorite) from the alteration halo related to unconformity-type uranium deposits. *Phys. Chem. Miner.* **2010**, *37*, 145−152.
(62) Mao, M.; Nilges, M. J.; Pan, Y. Single-crystal EPR and ENDOR study of an Al-O- center in prehnite: implications for aluminium-associated oxyradicals in layer silicates. *Eur. J. Mineral.* **2010**, *22*, 381−392.
(63) Bonin, J.; Lampre, I.; Mostafavi, M. Absorption spectrum of the hydrated electron paired with nonreactive metal cations. *Radiat. Phys. Chem.* **2005**, *74*, 288−296.
(64) Coudert, F.-X.; Boutin, A. Confinement effect on the hydrated electron behaviour. *Chem. Phys. Lett.* **2006**, *428*, 68−72.
(65) Fattahi, M.; Houee-Levin, C.; Ferradini, C.; Jacquier, P. Hydrogen-peroxyde formation and decay in gamma irradiated clay water. *Radiat. Phys. Chem.* **1992**, *40*, 167−173.
(66) Hensen, E. J. M.; Tambach, T. J.; Bliek, A.; Smit, B. Adsorption isotherms of water in Li-, Na-, and K-montmorillonite by molecular simulation. *J. Chem. Phys.* **2001**, *115*, 3322−3329.
(67) Boek, E. S.; Coveney, P. V.; Skipper, N. T. Monte Carlo molecular modeling studies of hydrated Li-, Na-, and K-smectites: Understanding the role of potassium as a clay swelling inhibitor. *J. Am. Chem. Soc.* **1995**, *117*, 12608−12617.
(68) Tay, K.; Boutin, A. Hydrated electron diffusion: the importence of hydrogen bonds dynamics. *J. Phys. Chem. B* **2009**, *113*, 11943−11949.
(69) Le Caer, S.; Lima, M.; Gosset, D.; Simeone, D.; Bergaya, F.; Pommeret, S.; Renault, J.; Righini, R. Dynamics of water confined in clay minerals. *J. Phys. Chem. C* **2012**, *116*, 12916−12925.
(70) Milosavljevic, B.; Thomas, J. Reactions of electrons on the surface of gamma-Al_2O_3. A pulse radiolytic study with 0.4 MeV electrons. *J. Phys. Chem. B* **2003**, *107*, 11907−11910.